A three-dimensional model of the boat–oars–rower system using ADAMS and LifeMOD commercial software

S Serveto[1]*, S Barré[2,3], J-M Kobus[2], and **J-P Mariot[1]**
[1]Laboratoire Motricité Interactions Performance, Université du Maine, Le Mans, France
[2]Laboratoire de Mécanique des Fluides, École Centrale de Nantes, Nantes, France
[3]École Nationale de Voile et des Sports Nautiques, Saint-Pierre Quiberon, France

The manuscript was received on 6 February 2009 and was accepted after revision for publication on 15 June 2009.

DOI: 10.1243/17543371JSET42

Abstract: This paper presents a numerical model of the boat–oars–rower system in a three-dimensional multibody dynamics approach using the ADAMS commercial software. The system is composed of four main parts: a skiff, two oars and a rower. The boat and oar mechanical model takes into account all boat settings and kinematic constraints, thus permitting a sophisticated model personalization. The rower skeletal model is built in LifeMOD (an ADAMS plug-in) software. In the example, a skilled rower is modelled with 19 human segments and 18 human joints which are personalized to the rower using the 32 external anthropometric data of the GEBOD program. In order to focus the tests on the rower on boat model, simulations are performed with basic hydrodynamic models for a single degree of freedom for the boat at first and then three degrees of freedom are used to show the potential of the model. The model is driven with five command signals, three oar rotations, seat movement, and lower torso rotation. The computed boat velocity is in good agreement with on-water measurements and a sensitivity test consisting of small variations of rowing technique allows the authors to be confident of the ability of the model regarding future optimization studies.

Keywords: multibody system, skeletal model, skiff, ADAMS, LifeMOD, GEBOD, optimization

1 INTRODUCTION

1.1 The benefits of the numerical simulation in optimizing the rowing performance

An elite rower is an athlete who has considerable muscular power and has also trained him/herself to manage that power in an optimal way, the performance criterion being the time duration for rowing 2000 m. Baudouin and Hawkins [**1**] in their analysis and Soper and Hume [**2**] in their literature review highlighted the parameters on which performance depends. To summarize, the mechanical and biomechanical key working parameters fit into three categories:

(a) the morphology and physical capacities of the rower;
(b) the oar settings and the rower installation in the boat;
(c) the rowing technique itself, i.e. the sequence and the proportioning of the muscle actions.

The parameters of the different categories are not independent and are correlated more or less strongly. Barrett and Manning [**3**] have exhaustively studied these parameters, their values, and their correlations. They showed that, for a skiff, the power developed by the rowers was the main factor influencing performance. Thus, the tallest and most powerful rowers are also the fastest and their settings arise from their morphologies. The results were obtained, however, with a sample of 15 rowers whose times over 2000 m have a standard deviation of 11.9 s. It is possible to therefore reverse the findings and suppose that athletes have similar power and morphology when the time intervals between their boats are in the order of a few seconds at the end of a race; then the question

**Corresponding author: Laboratoire Motricité Interactions Performance, Université du Maine, Avenue Olivier Messiaen, Le Mans, Sarthe, 72, France.*
email: sebastien.serveto@univ-lemans.fr

is how to improve the performance of elite rowers who have equivalent morphologies and energetic potential levels. To answer this question, a look at the factors less statistically correlated with performance becomes necessary; the optimization approach has to be more deterministic and consequently more individualized. Ultimately, the problem is the following: how to suggest to an elite rower, or to a crew, reliable indications for improving their performance by adjusting the boat and oar settings and the rowing technique.

It is impracticable to answer this question experimentally only with on-water tests because rowers need a long time to adapt their technique to new settings or installations [**4**, **5**]. That would require far too much availability of rowers in addition to the physiological risks. Another possibility consists in using numerical simulations in order to identify some reliably optimized sets of parameters and thus limit the on-water tests to validate these parameters. This was the original method chosen. Since the objective was to improve the performance of elite rowers, who by definition are already close to the optimum, the approach using numerical simulations would be relevant only if the complete system 'boat + oars + rowers' was accurately modelled.

1.2 Evolution of simulations: from one-degree-of-freedom boat motion toward three degrees of freedom (and more)

Propulsion by oars naturally produces an unsteady and cyclic behaviour of the system. The most apparent characteristic is the significant boat velocity fluctuation which makes the hydrodynamic and aerodynamic phenomena more complex. The problem can be described by starting with the expression of the fundamental principle of mechanics written with one degree of freedom along the surge axis [**6**]. This one-degree-of-freedom equation is sufficient to see that the fields of mechanics (boat and oars), biomechanics (oarsman), and fluid mechanics (water and air interaction) are involved in the performance. Indeed, the scientific publications in each one of these fields have been very prolific in recent years.

Many authors perform simulations by solving the one-degree-of-freedom equation, generally for a skiff. The results given by this simple model [**6**–**10**] confirm that the velocity unsteadiness is generated first by the intermittent propulsion forces and second by the movement of the rower on the boat. This unsteadiness has a significant influence on dissipated energy and thus on efficiency [**11**]. It could also be interesting to take into account the lack of performance caused by the boat's secondary movements (mainly pitching, heave, and yaw). Hydrodynamic resistance is influenced by these movements, which also directly cause a dissipation of energy because of hydrodynamic damping (wave radiation and viscous dissipation). To estimate the influence of boat behaviour on performance the movements have to be calculated by solving the coupled equations of mechanics on all the degrees of freedom. From a practical point of view, the writing of the system of equations is elaborate when the number of degrees of freedom increases, but this is not the worst problem. The difficulty is to develop consistent models to calculate the unsteady hydrodynamic loads. Several attempts have been made in this area by hydrodynamic specialists. In recent works, Formaggia *et al.* [**12**] took into account the pitch and heave movement and showed that the energy dissipated by the secondary movements accounts for approximately 10 per cent of all dissipated energy. They developed a 12-segment model using the MIST program of NASA to estimate the mass segments, angular inertia being neglected. This body model was exploited to drive simulations with up to four rowers on a boat moving with three degrees of freedom (surge, heave, and pitch). This feature imposed the calculation of suitable hydrodynamic coefficients to obtain the fully coupled hull–rower system behaviour. A resolution of the unsteady hydrodynamic problem for one degree of freedom and three degrees of freedom, using the non-linear RANSE computational fluid dynamics (CFD) code with free water surface, was suggested in references [**13**] to [**15**]. Given the complexity of the flows around the oar blades, the modelling of the hydrodynamic loads on the oars also remains a topical question [**16**, **17**]. In this respect, progress is being made in computing unsteady loads on blades with CFD code [**18**, **19**].

To be fully exploited in the future, progress in hydrodynamic and aerodynamic modelling must be accompanied by a parallel improvement in boat + oars + rower mechanical and biomechanical modelling. In particular, the modelling of the displacement of the rower mass centre in all directions and the rower inertial moments is absolutely necessary for accurate calculation of the excitation loads in surge, heave, and pitch. Those considerations will probably lead to the generalized development of three-dimensional (3D) mechanical models.

1.3 Reasons for using commercial software

Owing to a large mass ratio, the rower's movement produces important inertial forces and moments which influence the velocity variations of the boat already induced by the intermittent propulsive forces. The rower's technique, the movements of the body segments, and the displacement of the rower's centre of mass are strictly linked. It is easy to understand why all the authors who propose rowing

simulators are seeking to refine the oarsman body modelling [**10**, **12**]. They rightly expect better relevance of the working analysis from this modelling. A complex biomechanical model of a rower has already been developed. Hase and colleagues [**20–23**], for example, evaluated mass and inertia characteristics of segments [**24**] and developed a 3D musculo-skeleton with 13 rigid segments. They added 32 muscles to understand the biomechanical activity and risks in rowing for fitness. Since the study considered the rower on an ergometer, however, the behaviour of the rower was not coupled with a boat movement.

When the rowers are on a boat moving not only in translation but with six degrees of freedom, the writing and the solving of the mechanical model of the boat coupled with a biomechanical model of the rowers becomes complicated. This is why the realization of a 3D model of the whole system was undertaken using commercial software. The technical benefit of such a solution is a powerful calculating and graphic facility which does not require the writing of mechanical equations for building the model and for each change in the model (number of rowers, number of elements, number of degrees of freedom, etc.). This kind of model can be modular and able to incorporate progress in aerodynamic and hydrodynamic modelling. It can also be interfaced with parametric optimization codes.

The task is to merge an advanced biomechanical model of a human body and a mechanical model of boat and oars in the same software environment. The attempt presented here treated the simplest configuration, i.e. a system composed of four main subsystems: a skiff, two oars, and a rower. In order to focus the tests on the rower-and-boat mechanical model, some simulations were carried out with basic hydrodynamic models and only three degrees of freedom for the boat.

2 THE BOAT + OARS + ROWER MODEL

2.1 Boat-and-oars mechanical model

The boat-and-oars mechanical model was developed by means of the mechanical modeller ADAMS (MD 2008 R3), which works with a Lagrangian formalism. The advantage of using ADAMS was to avoid elaborate mechanical calculations.

The boat components were modelled as rigid solids. Each real mechanical element was specified in terms of its mass and inertia matrix. To include flexible elements is possible (oars, for example), but this feature was not used. The 3D mechanical system boat + oars is presented in Fig. 1. The origin of the boat reference frame (O_B) was located at the front upper point of the seat when this point was lying in the vertical transverse plane containing the rowlock pins. As shown in Fig. 1, the oar kinematics took into account the relative position of the different rotational axes of the rowlocks.

The model could be adjusted for different rower morphologies. The setting parameters were those used on competition boats. To adjust these parameters, some reference points were localized in the boat reference frame:

(a) the rowlock pins reference points;
(b) the foot stretcher reference point as shown in Fig. 1.

The feet and the hands of the rower were attached at a nominal position on the foot stretchers and on the oar handle, respectively. The principle for installing the rower in the boat was based on virtual and massless setting devices. These devices were built with suitable joints which permitted translations and rotations depending on their type.

This principle was applied for setting the position and the angle of the foot stretcher, the angle of the seat slides, the rowlock, and the oars. It was possible to adjust l_{in}, the effective inner lever and l_{out}, the effective outer lever with two sliding joints and the centre of mass and the inertia of the oars were automatically modified. The lever arms l_{in} and l_{out} are defined in Fig. 1. The virtual setting devices could eventually be driven during the simulation like the other commands without interrupting the simulation. Table 1 gives the adjustable parameter values introduced into the personalized model. These values were measured on the boat of the rower which was modelled for the presented simulations.

To simulate the movement of the boat on the water a six-degree-of-freedom virtual joint was adopted whose degrees of freedom could be blocked according to the aim of the simulation. The greater the number of degrees of freedom, the more relevant the knowledge of hydrodynamics coefficients. This point will be discussed later.

2.2 Rower biomechanical model

The biomechanical model of the rower was developed with the ADAMS plug-in LifeMOD. The positions and inertial parameters of the body segments and the joint locations were generated by the GEBOD (GEnerator of BOdy Data). Using regression equations, GEBOD could generate automatically 32 external anthropometric measures from four input parameters (age, weight, height, and gender). The direct inputting of these 32 measures was preferred in order to personalize the model of the rower. The measurement protocols and the geometric models used in GEBOD are detailed by Cheng *et al.* [**25**, **26**]. Table 2 gives the 32 anthropometric measurements used to generate a personalized model with 19 body segments and 18 human joints (Fig. 2).

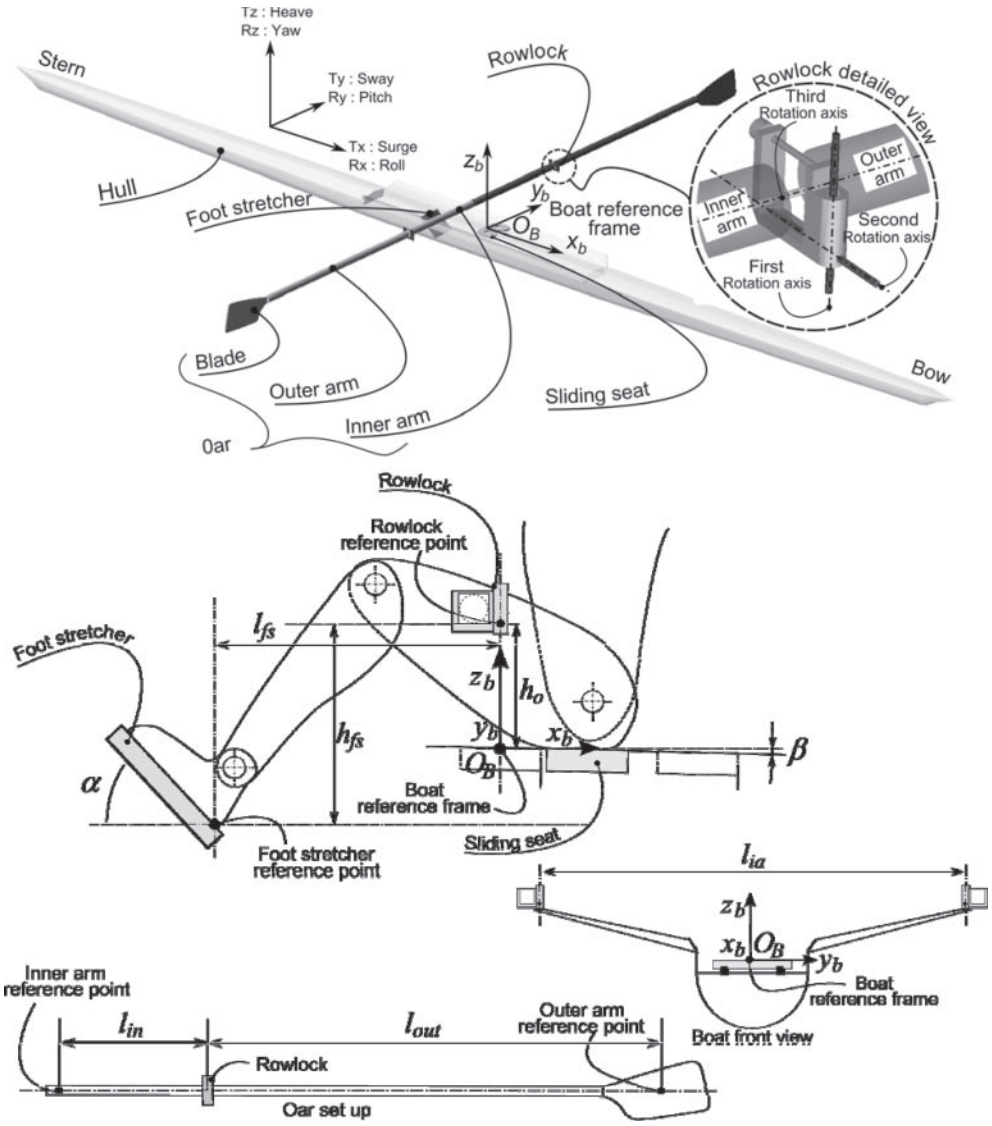

Fig. 1 Main parts of the 3D skiff model, reference frame, and adjustable set-up. The rowlock detailed view shows the different rotation axes. The adjustable parameters were: h_o the rowlock height, h_{fs} the foot stretcher height, l_{fs} the foot stretcher longitudinal position, l_{in} the inner arm lever length, l_{out} the outer arm lever length, l_{ia} the inter axes distance, α the foot stretcher angle, and β the slide angle

Table 1 Values of the personalized model

Parameters	Values	Parameters	Values
h_o	17 cm	l_{fs}	37 cm
h_{fs}	33 cm	l_{in}	85 cm
l_{ia}	160 cm	l_{out}	183.7 cm
α	45°	β	0°

Each human joint was built with three revolute joints, each of which corresponded to one degree of freedom. The number and the choice of the degrees of freedom of each joint depended on the nature of the human joint (example: knee = one degree of freedom; shoulder = three degrees of freedom).

2.3 Mechanical mutual actions

The mechanical actions exerted by the subsystem 'rower + sliding seat + oars' on the boat were composed of gravitational effects (static contribution) and inertial effects (dynamic contribution)

$$\begin{aligned} \boldsymbol{F} &= \boldsymbol{F}_{\mathrm{S}} + \boldsymbol{F}_{\mathrm{D}} = m\,\boldsymbol{g} + m\,\boldsymbol{a}_G \\ \boldsymbol{T}_{(O_{\mathrm{B}})} &= \boldsymbol{T}_{\mathrm{S}(O_{\mathrm{B}})} + \boldsymbol{T}_{\mathrm{D}(O_{\mathrm{B}})} = \boldsymbol{O_B G}\times m\,\boldsymbol{g} + \boldsymbol{T}_{\mathrm{D}(O_{\mathrm{B}})} \\ &\quad + \boldsymbol{O_B G}\times m\,\boldsymbol{a}_G \end{aligned} \tag{1}$$

with $\boldsymbol{F}_{\mathrm{S}}$ and $\boldsymbol{T}_{\mathrm{S}}$ being the static force and torque contribution, $\boldsymbol{F}_{\mathrm{D}}$ and $\boldsymbol{T}_{\mathrm{D}}$ the dynamic force and torque contribution, m the subsystem mass, $\boldsymbol{a}_G$ the subsystem centre of mass acceleration, $\boldsymbol{g}$ the gravity

acceleration, O_B the boat reference frame centre and G the subsystem mass centre.

2.3.1 Hand–oar mechanical actions

Mechanical links between hands and oars were built in two steps.

1. A revolute joint was added to the handle of each oar in order to permit the free rotation of the oar shaft in the handle.
2. A 3D viscoelastic joint was defined between the hand and the oar handle (see Fig. 3).

Table 2 The 32 anthropometric measurements data used to personalize the rower model

Measurements	Value	Measurements	Value
Weight	89.2 kg	Hip breadth standing	34.1 cm
Standing height	182 cm	Shoulder to elbow length	41.5 cm
Shoulder height	151.8 cm	Forearm–hand length	49.5 cm
Armpit height	137.2 cm	Biceps circumference	34.5 cm
Waist height	112 cm	Elbow circumference	33 cm
Seated height	92 cm	Forearm circumference	30.5 cm
Head length	21 cm	Waist circumference	18.5 cm
Head breadth	15.8 cm	Knee height seated	58 cm
Head to chin height	23 cm	Thigh circumference	61.5 cm
Neck circumference	38 cm	Upper leg circumference	41.5 cm
Shoulder breadth	48.3 cm	Knee circumference	42 cm
Chest depth	25.6 cm	Calf circumference	40.5 cm
Chest breadth	34.3 cm	Ankle circumference	25.5 cm
Waist depth	22.8 cm	Ankle height, outside	11.5 cm
Waist breadth	29.7 cm	Foot breadth	10.5 cm
Buttock depth	27 cm	Foot length	28.5 cm

Let R_{oh} and R_h be respectively the frame of reference of the oar handle and hand. Let x, y, and z be the coordinates of O_h expressed with respect to R_{oh}. Let θ_x, θ_y, and θ_z be the characteristic orientation angles of R_h with respect to R_{oh}. The mutual mechanical actions between the hand and the handle were defined as an isotropic model for the generalized efforts ($\boldsymbol{F}_h$, $\boldsymbol{T}_h$) given by

$$\boldsymbol{F}_h = \left\{ \begin{array}{l} F_x = K_T x + C_T \dot{x} \\ F_y = K_T y + C_T \dot{y} \\ F_z = K_T z + C_T \dot{z} \end{array} \right\}$$
$$\boldsymbol{T}_h = \left\{ \begin{array}{l} T_x = K_R \theta_x + C_R \dot{\theta}_x \\ T_y = K_R \theta_y + C_R \dot{\theta}_y \\ T_z = K_R \theta_z + C_R \dot{\theta}_z \end{array} \right\} \quad (2)$$

where F_x, F_y, F_z and T_x, T_y, T_z were forces and torques components, respectively, K_T and C_T being the translational stiffness and damping isotropic coefficients and K_R and C_R being the rotational stiffness and damping coefficients. Owing to the handle rotational degree of freedom around $\mathbf{y}_{oh}$, the T_y component was null.

2.3.2 Foot–foot stretcher mechanical actions

Mechanical links between feet and foot stretcher were modelled by 3D viscoelastic joints located

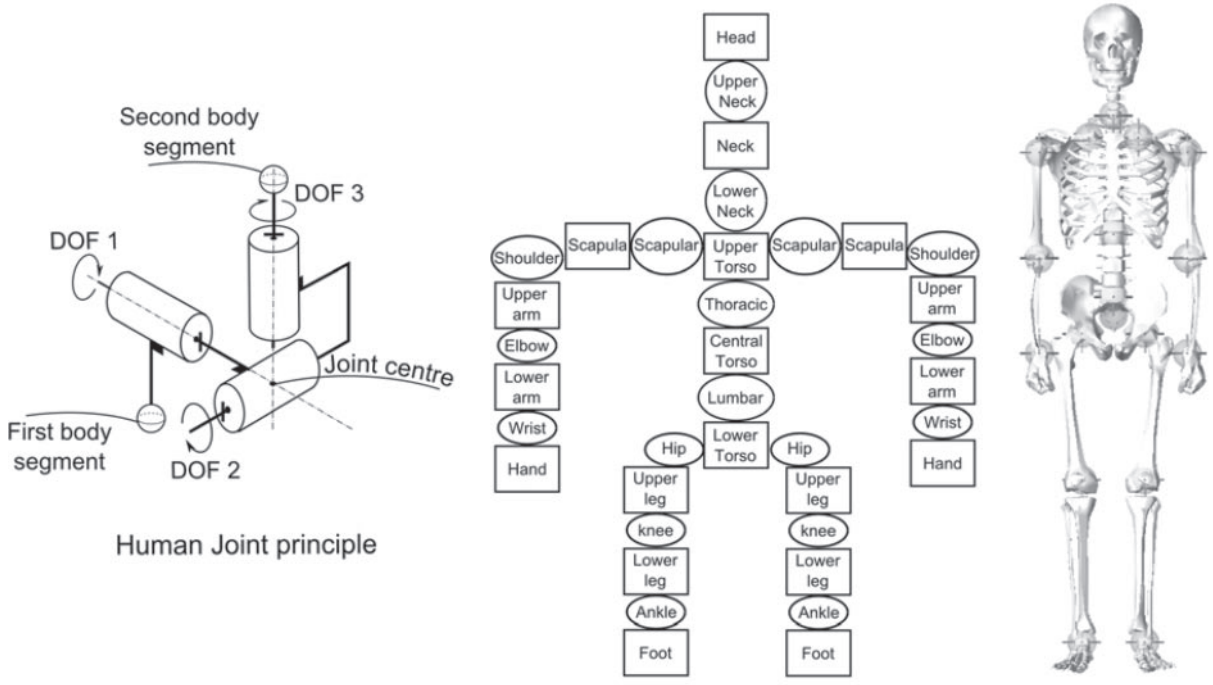

Fig. 2 The left diagram shows the human joint principle used in LifeMOD. All the joints were composed of three revolute mechanical joints, each one associated with one degree of freedom. The middle diagram presents the 19 human segments and 18 human joints generated by GEBOD in LifeMOD and the right diagram shows the representation of the generated skeletal model

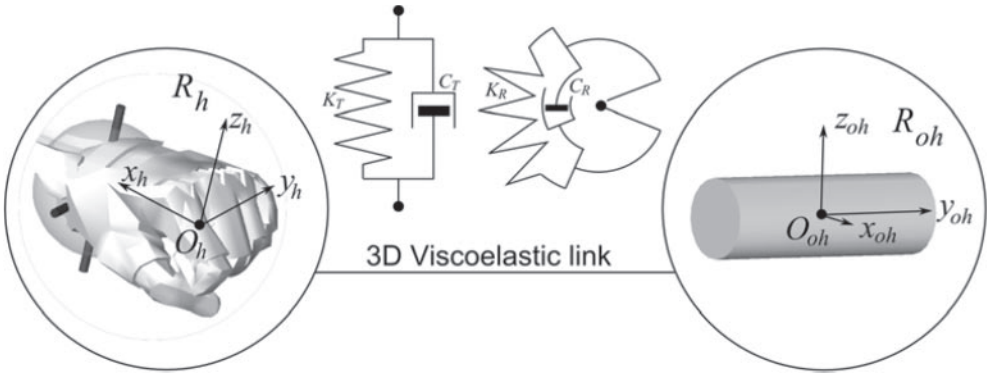

Fig. 3 The oar handle and the hand were linked by a 3D viscoelastic joint. The viscoelastic joint was defined by translational and rotational stiffness and damping between the centre hand fixed frame R_h (O_h, [$\boldsymbol{x}_h$, $\boldsymbol{y}_h$, $\boldsymbol{z}_h$]) and the centre oar handle fixed frame R_{oh} (O_{oh}, [$\boldsymbol{x}_{oh}$, $\boldsymbol{y}_{oh}$, $\boldsymbol{z}_{oh}$])

between metatarsus number 2 and its first associated toe. This point corresponded to the limit of the fore part of the shoes effectively attached to the foot stretcher. This feature allowed the heels to rise from the foot stretcher.

2.3.3 Lower torso sliding seat mechanical actions

The mechanical link between the sliding seat and the lower torso was a 3D viscoelastic joint at the seat level and a revolute joint around the axis defined by the line passing through the two femoral articulations. This revolute joint allowed the lower torso to rotate on the sliding seat. It was located at a vertical distance from the sliding seat corresponding to the gluteus muscle thickness. This feature permitted differentiation between the seat and hip movements owing to the rotation of the rower trunk.

3 HYDRODYNAMIC MODEL

The aim of the presented simulation was to demonstrate the ability of the mechanical model to work with three degrees of freedom, and the modelling of the hydrodynamic efforts acting on the hull and on the oars was drastically simplified. The following sections detail the hypothesis and simplification. At this first stage, only the surge, heave, and pitch degrees of freedom of the boat were considered, the other degrees of freedom being blocked. Table 3 gives the numeric values of the hydrodynamic parameters used in the model to simulate the behaviour of a skiff. It can be seen that aerodynamic drag was neglected.

3.1 Hydrostatic and wave radiation forces

Only the main components of the hydrostatic stiffness, added masses, and wave radiation damping were taken into account. The coupled components were neglected in view of the quasi-symmetry of the hull. The surge wave radiation damping and the nonlinear heave and pitch damping were also neglected. Considering that the gravity forces and buoyancy forces were balanced at rest, the components $F_{\mathrm{WB}x}$, $F_{\mathrm{WB}z}$, and $T_{\mathrm{WB}y}$ (WB stands for water on boat) of forces and torque acting on the hull were reduced to

$$\begin{aligned} F_{\mathrm{WB}x} &= -R - Am_{xx}\,\ddot{x}_{\mathrm{B}} \\ F_{\mathrm{WB}z} &= -K_{zz}\,z_{\mathrm{B}} - D_{zz}\,\dot{z}_{\mathrm{B}} - Am_{zz}\,\ddot{z}_{\mathrm{B}} \\ T_{\mathrm{WB}y} &= -K_{\theta\theta}\,\theta - D_{\theta\theta}\,\dot{\theta}_{\mathrm{B}} - AI_{xx}\,\ddot{\theta}_{\mathrm{B}} \end{aligned} \tag{3}$$

where R is the resistance (>0). K_{zz} and $K_{\theta\theta}$ are the hydrostatic stiffness about z_{B} (heave) and θ_{B} (pitch), respectively. They were estimated from the hull charcteristics of the skiff. Considering the small amplitude of the movements, the stiffness coefficients were considered to be constant. D_{zz} and $D_{\theta\theta}$ are the linear damping coefficients owing to wave radiation and Am_{xx}, Am_{zz}, and AI_{xx} are the added masses and added inertia in surge, heave, and pitch, respectively.

Plausible values of added mass and damping hydrodynamic coefficients of the skiff were obtained by applying the Froude similitude law to the coefficients calculated by Formaggia *et al.* [**12**] for a four-rower boat. The scale factor for length was 1.6, the cubic root of the weight ratio assumed to be four. The numeric values of hydrodynamic parameters of the model are given in Table 3.

Table 3 Numerical values of the hydrodynamic parameters

Parameters	Values	Parameters	Values
ρ	10^3 kg/m^3	L_{w}	8 m
ν	10^{-6} m^2/s	S_{b}	0.11 m^2
C_{n}	1.8	S_{w}	2 m^2
K_{zz}	17 000 N/m	$K_{\theta\theta}$	80 000 Nm/rad
D_{zz}	350 N/m s	$D_{\theta\theta}$	1120 Nm/rad s
Am_{xx}	2 kg	Am_{zz}	55 kg
AI_{xx}	150 kg m^2		

3.2 Hydrodynamic resistance of hull

Although it is an approximation [**13–15**], a quasi-static approach was used for calculating the hydrodynamic resistance. That is sufficient for the purpose of this article. Thus, the resistance was assumed to depend only on the hull velocity component $V(t)$ and could be estimated (by measurements or CFD calculations) at each time t as if the velocity was steady. Here, the resistance was calculated according to the recommendations of the International Towing Tank Conference (ITTC) [**27**], so the hydrodynamic force on the hull was expressed by

$$R = 1/2\rho\, S_{0w}\, C_T\, V(t)^2 \tag{4}$$

where C_T is the total resistance coefficient expressed by

$$C_T = C_f(1+k) + C_W \tag{5}$$

where ρ is the water density, S_{0w} the nominal wetted surface of the hull (at rest), C_f the friction coefficient, $V(t)$ the boat velocity at the instant t, k a form factor, and C_W the wave resistance coefficient. The form factor and the wave resistance coefficient were estimated from tests of a skiff at full scale carried out in the towing tank of the Ecole Centrale de Nantes [**28**]. The form factor was evaluated at 0.14 using the Prohaska procedure [**27**] and the wave resistance was about 8.5 per cent of the friction resistance at the mean velocity reached in the simulation presented in this paper. This gave a total resistance of $R = 1.2\ R_f$. The ITTC formula

$$C_{f\,ITTC} = 0.075/(\log_{10} Re - 2)^2 \tag{6}$$

was assumed to be valid at each time, with

$$Re = Re(t) = V(t)L_w/\nu \tag{7}$$

where L_w and ν are the boat wetted length and the kinematic viscosity of the water, respectively. Some authors [**12**, **29**] have also used this formula to estimate the friction resistance. This was an approximation because the boundary layer around the hull is highly perturbed by the large surge motion of rowing boats.

3.3 Hydrodynamic force on oar blades

It is not the intention at this stage to incorporate in the simulation a sophisticated model for the force on the oar blade. Moreover, to model this force accurately, it is necessary to take into account the blade immersion [**19**], the blade angle with the shaft, the vertical blade angle, the variation of the application point of the force, the oar deformation, and the unsteady characteristics of the blade movement. This model is currently under development and will be used when completed. In this paper, the model used is the basic model of Wellicome [**16**]. It is a simplified model which considers that the force is normal to the blade. This effort is applied at the blade centre on the oar arm axis and at a distance l_{out} of the rowlock pin. It is given by

$$F_{WO}(t) = 0.5\,\rho\, S_b\, C_n V_n^2(t)\ \boldsymbol{e}_n \times \boldsymbol{e}_{x0} \tag{8}$$

with S_b being the blade surface area, C_n is the normal force coefficient, V_n is the normal component of the blade centre velocity, $\boldsymbol{e}_n$ and $\boldsymbol{e}_{x0}$ are the unit vector of the normal to the blade and the unit vector of the displacement direction in the Galilean frame on reference. The value of the C_n coefficient was roughly estimated using the results of tests carried out with a big blade oar at full scale in a towing tank [**28**].

4 SIMULATION TEST

4.1 Reconstructed rower kinematics and input data to control the model

In general, human biomechanics models are controlled by joint coordinates experimentally and largely derived from ergometers and optoelectronic devices [**10**, **12**, **17**]. These kinds of data are not available for on-water measurements. To overcome this problem, another approach was adopted. In this approach the rower kinematics was reconstructed from boat kinematics consisting of rowlock angular rotation and in-boat sliding seat displacement.

Consequently, the skeletal model was rendered passive with the introduction of stiffness and damping at each rower joint. Rower kinematics were then adjusted by varying the joint stiffness and damping coefficients. These coefficients can be considered as weighting factors for joint angular amplitude. Indeed, the greater the stiffness and damping, the smaller the amplitude. The realistic character of the obtained kinematics was established according to the trainer and rower expertise. It must be noted that this expertise could not be possible without 3D animation.

Boat kinematics were partially derived from on-water measurements, rowlock pin angle, and sliding seat displacement. These measurements had been obtained with the modelled rower on an instrumented skiff (see Appendix) at a training rate of 18 strokes per minute (spm). Using a Fourier treatment, these two measurements were smoothed to obtain perfectly periodic signals. To complete the boat kinematics, three other data were derived according to expert background; they consisted of the other two oar rotations and lower torso rotation with respect to the seat. Also, the head was constrained to a translational motion in the sagittal plane, the rower continuing to look in the surge direction.

All these digital signals were transformed into cubic splines for ADAMS inputs, as shown in Fig. 4, where the time was scaled in percentages of the stroke period.

4.2 Results

The results presented are not intended to be directly interpreted but they are representative of the potential of the merged mechanical and biomechanical models. The simulations were performed at a rate of 18 spm corresponding to the stroke rate of the on-water measurements. The results corresponded to the model behaviour after obtaining a stabilized rowing cycle. Two simulations were performed, the first one with only the surge degree of freedom of the boat and the second one with three degrees of freedom, i.e. surge, heave, and pitch.

4.2.1 One-degree-of-freedom simulation

In the presented simulation, the rower motion only influences the velocity in the x-direction because five degrees of freedom of the boat were fixed. The boat moved as if it were guided by a translational joint in the x-direction. The 3D mechanical model, however, allows the computation of the six components of the fluctuating loads generated by the rower motions in the boat. Figure 5(a) shows the rower mass centre displacement in the boat. This is one of the principal elements which characterize the rower's technique. Owing to the symmetric input data of the model, the rower mass centre lies in the $(O_B, [x, z])$ plane. The amplitude of the rower mass centre is 0.69 m in the x-direction and 0.1 m in the z-direction. This amplitude of motion in the x-direction was higher than the sliding seat motion, which is only 0.53 m. This difference in amplitude and this behaviour underlined the reason to model the rower body accurately.

The mechanical actions exerted by the subsystem rower + seat + oars are given in Fig. 5(b). They were composed of gravitational effects (static contribution) and inertial effects (dynamic contribution). Owing to the model symmetry characteristics only F_x, the efforts along x (surge motion excitation), F_z, the effort along z (heave motion excitation), and T_y, the torque around y (pitch motion excitation), were not

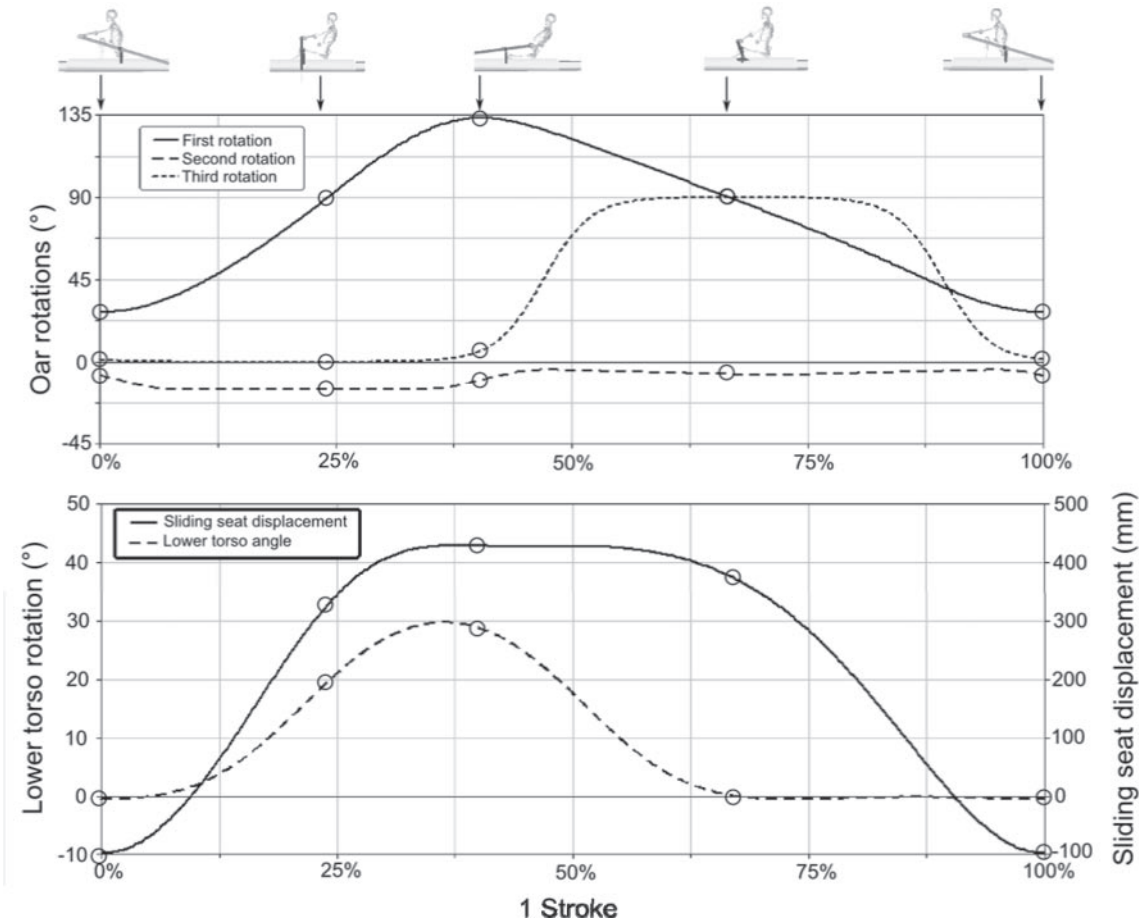

Fig. 4 Data introduced as cubic splines to control the kinematics of the model. Upper curves represent the three rotations of oar controlling the oar motion at rowlock level. Lower curves represent the lower torso rotation and the seat displacement

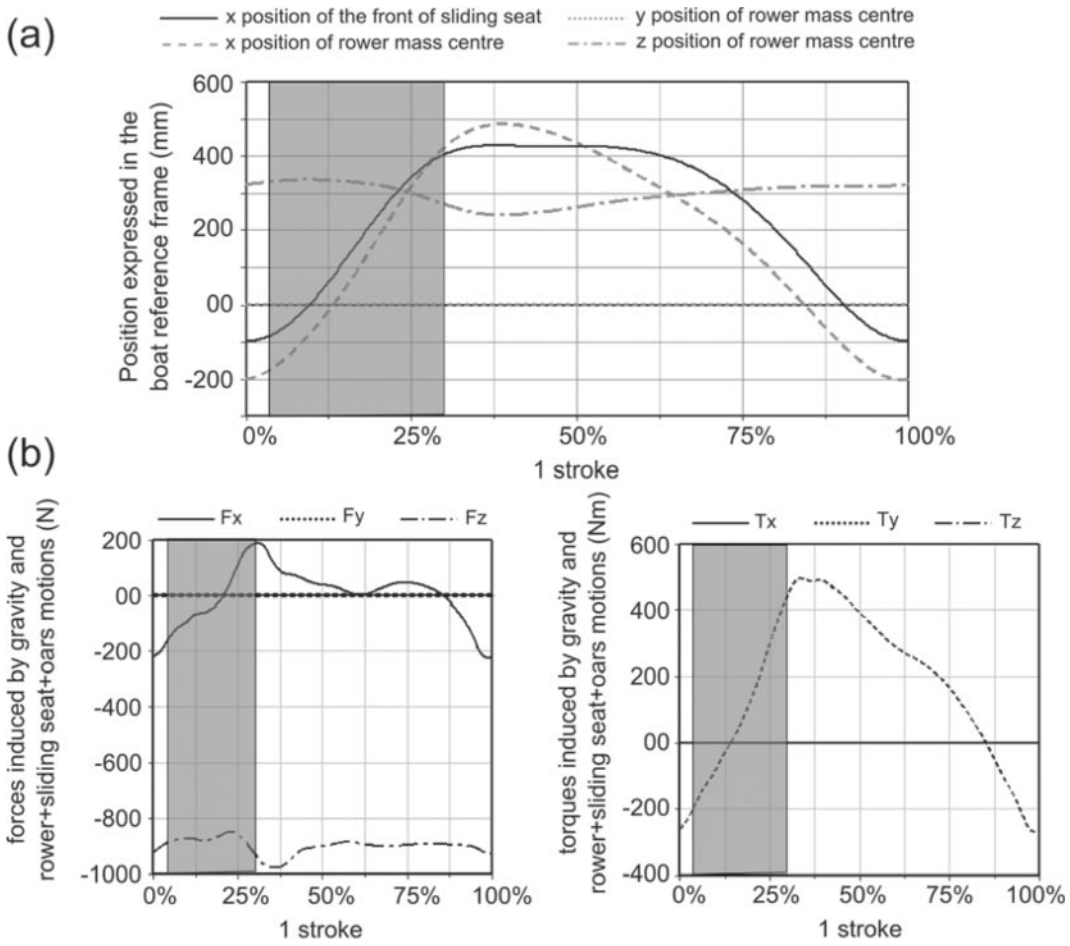

Fig. 5 The one-degree-of-freedom surge simulation at 18 spm. (a) Rower mass centre displacement and sliding seat displacement during one stroke. The coordinates were expressed in the boat reference frame. (b) Mechanical actions applied on boat by the subsystem rower + sliding seat + oars. The forces and torques applied by the subsystems were expressed in the boat reference frame. The torques were calculated at O_B the origin of the boat reference frame. The shaded areas indicate the hydrodynamic propulsive phase

zero. The force F_x varied between +200 and −230 N, F_z varied between −855 and −980 N, and T_y varied between 500 and −270 Nm.

Figure 6(a) presents the results for the boat velocity. It appeared that the propulsive hydrodynamic effort vanished before the velocity peak. In fact, close to the peak at 30 per cent of the total stroke duration, the acceleration of the boat was only caused by rower inertial contribution (see F_x component in Fig. 5(b)). This result confirmed an observation well known to the rowing community. Figure 6(b) compares the boat velocity computation with measured data. The measured mean velocity is 3.35 m/s compared with 3.22 m/s for the simulated mean velocity.

As the model will be used for the optimization of the rower technique, its sensitivity when modifying a parameter of the technique must be tested. As an example, Fig. 7 shows the sensitivity of the model with respect to the rower lower torso rotation. The amplitude of this rotation influenced the velocity profile and consequently the mean velocity as shown in Table 4. The more the rower launches backward, the higher the mean velocity. The relative increase was 2.1 per cent when the lower torso rotation angle varied from 0° to 30°. Notice that such an exaggerated variation was applied to test the sensitivity of the model but is not realistic for biomechanical reasons.

To confirm the interest of a multi-segment rower model [**10**, **12**], the boat velocity was also computed using a single equivalent mass fixed on the sliding seat. This is shown in Fig. 7 with a different velocity behaviour leading to a smaller velocity.

4.2.2 Three degrees of freedom simulation

Figure 8 shows the calculated secondary movements with the periodic commands used for the one-degree-of-freedom simulation. They were compared with the same movements derived from on-water measurements (see Appendix) during an equivalent temporal sequence. The comparison was not easy

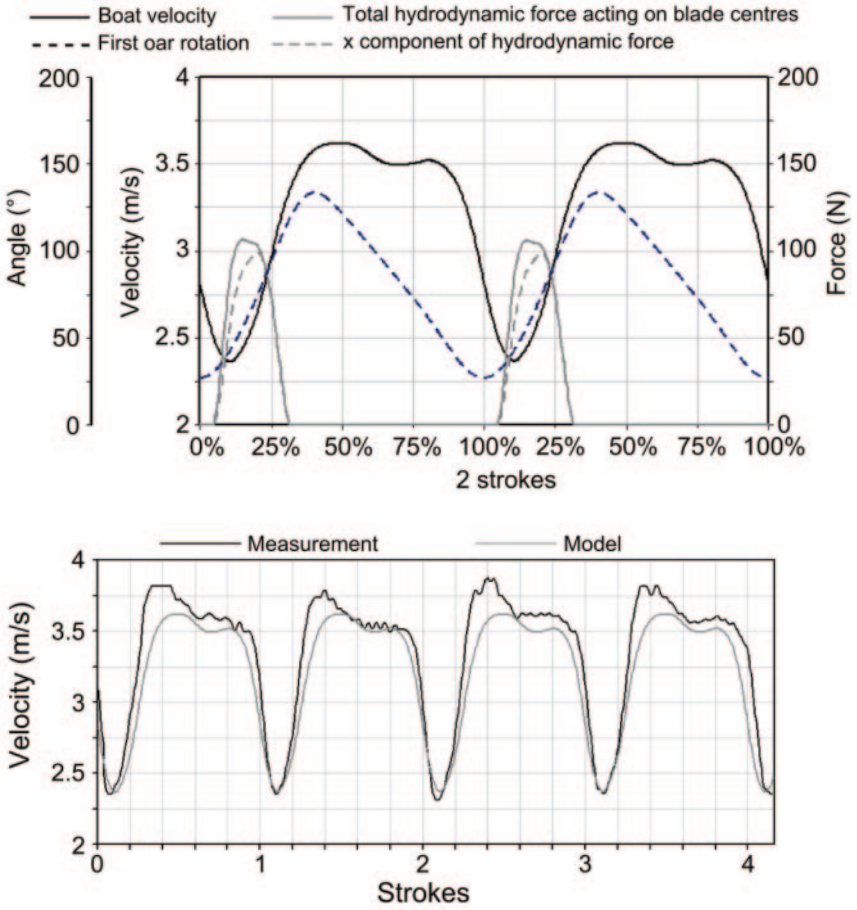

Fig. 6 (a) One-degree-of-freedom simulation at 18 spm: results for hydrodynamic forces and boat velocity. (b) Comparison between calculated and measured velocity of the boat

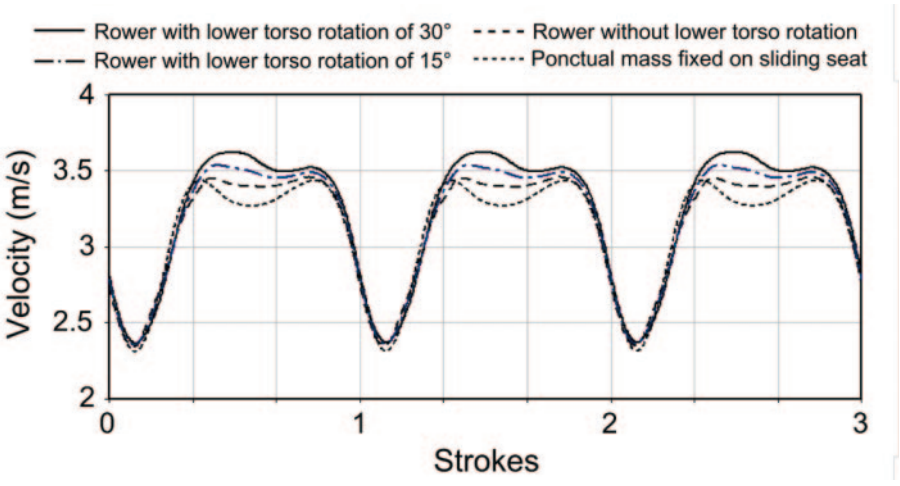

Fig. 7 Model sensitivity to change of technique parameter. The parameter tested here was the magnitude of the rower lower torso rotation at 18 spm

because the measured data were not perfectly periodic. The pitch amplitude was well reproduced but the heave is damped in comparison with the measured movement. The hydrodynamic coefficients of wave radiation (added masses and damping), derived from the results of Formaggia *et al.* [**12**], were calculated at the stroke rate considered as the fundamental frequency of the movement. Given the

excitation efforts plotted in Fig. 5, this hypothesis was justified for pitch but the heave excitation appeared to be a transient one at the release. Thus, the frequency of the main component of the heave response is manifestly higher and probably near the natural frequency after the excitation. Since the hydrodynamic coefficients depend on frequency, the added mass and damping of heave are not evaluated very well. It can be seen that the main frequencies of heave are not the same. This fact shows clearly the limit of the harmonic approach of the radiation problem for rowing and the convolution approach will be preferred in the future. Since the coupled hydrodynamic coefficients were neglected and the influence of the secondary movements on the resistance was not taken into account, the boat velocity is weakly modified by the secondary movements. This is another point which must be accounted for.

Table 4 Mean velocity versus lower torso rotation angle

	Mean boat velocity (m/s)			
	3.22	3.19	3.15	3.12
Lower torso rotation angle (deg)	30	15	0	Equivalent mass point on seat

4.2.3 Visualization and animation

The powerful graphic interface of ADAMS is a feature that has to be discussed with the coaching staff and rowers. For example, Fig. 9 shows an instantaneous picture picked up during an animation and shows the possibilities offered by the ADAMS environment to render visually the calculated results, particularly the well known and typical absolute motion of the blade centre [**17**].

5 DISCUSSION

The level of agreement between the computed results and the measured data gives credence to the methodology and the realism of the model.

The release degree of freedom in the model is not a mechanical problem when a powerful mechanical modeller such as ADAMS-LifeMOD is used but it

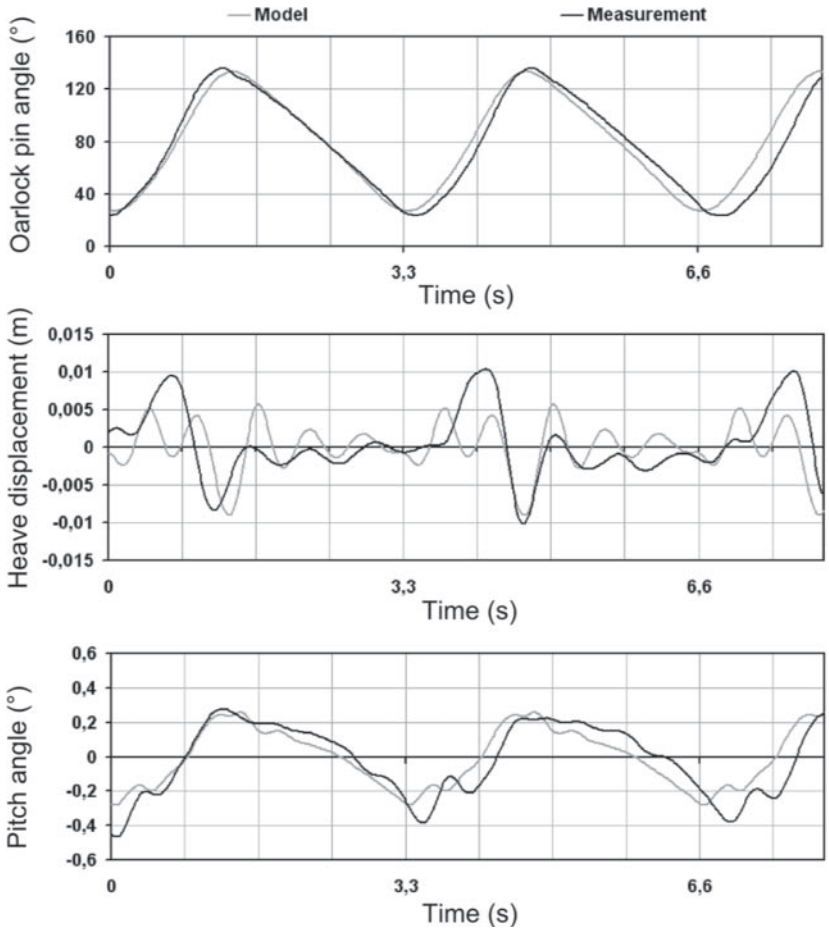

Fig. 8 Comparisons between calculation and measurements for heave and pitch movements. Above the rowlock signals are used to synchronize measurements and calculations

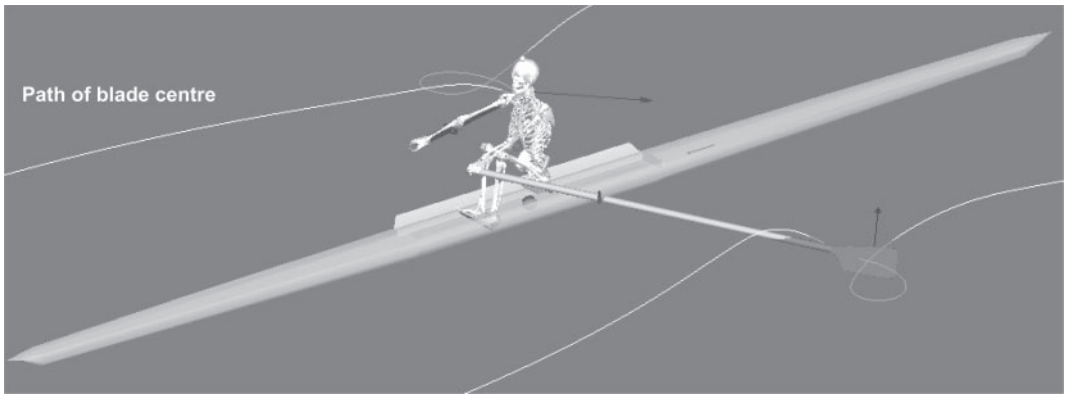

Fig. 9 3D visualization of the global model kinematic. Picture from 3D animation obtained with the ADAMS postprocessor

needs to integrate a more complex set of hydrodynamic coefficients to take into account the water actions. The results presented in this paper show the possibilities offered by this model in terms of optimization. The goal for future study will be to use this model as a relevant tool for determining sets of optimized parameters.

6 CONCLUSION

Special attention was given to the biomechanical model of the rower and to the multibody model of the boat, the main reason being that a well-defined 3D mechanical model of the rower and the boat constituted the necessary first stage to obtain relevant estimations of instantaneous velocity and secondary movements. The decision to develop the coupled models in a specialized commercial software environment avoided the need to write mechanical equations when the mechanical elements of the system became quite numerous.

The rower's skeletal model was built in LifeMOD. It is composed of 19 human segments and 18 human joints and can be personalized with 32 external anthropometric data.

ADAMS allowed a multibody dynamic model of the boat equipped with virtual setting devices to be built, which allowed the model to match any rower morphologies. The rowlock kinematics were modelled with a high degree of realism, taking into account the three non-concentric rotational axes. Moreover, all kinematical joints were considered as perfect joints without friction and the oars as rigid bodies. It should be noted that friction and flexible oars could be introduced to obtain more parameters for optimization studies.

Although the hydrodynamic models used here for the boat/water and blade/water interactions were simplified at this preliminary stage, the model of the whole 3D system includes all the fields involved in rowing: mechanics, biomechanics, and hydrodynamics. The simulations carried out aimed at showing the possibilities offered by the oar + boat + rower model. The method of driving the model was adopted in order to test the model with few kinematic inputs at rowlock and sliding seat. Thus, the rower was considered as a passive system with adjustable rotational stiffness and damping at each human joint. The human joint stiffness and damping coefficients were chosen according to trainer expertise to obtain realistic rower kinematics. This method was not adapted for detailed analysis of rower technique or to propose relevant optimization parameters. For that, the rower's technique has to be precisely analysed before being correctly introduced into the model. Before the model is used for rowing optimization, the priority is to build a parametric modeller of the rowing technique.

ACKNOWLEDGEMENTS

This study was carried out within the project OPERF2A supported by the Region des Pays de la Loire as part of the research programme on rowing jointly developed by the French Rowing Federation (FFSA), the Ecole Centrale de Nantes, and the Ecole Nationale de Voile et des Sports Nautiques (ENVSN) and supported by the French Ministry of Sports (MSJSVA). The authors express their thanks for the collaboration of the rowers and trainers of the Pôle France Aviron of Nantes.

REFERENCES

1 **Baudouin, A.** and **Hawkins, D.** A biomechanical review of factors affecting rowing performance. *Br. J. Sports Med.*, 2002, **36**, 396–402.

2 **Soper, C.** and **Hume, P. A.** Towards an ideal rowing technique for performance, the contributions from biomechanics. *Sports Med.*, 2004, **34**, 825–848.
3 **Barrett, R. S.** and **Manning, J. M.** Relationships between rigging set-up, anthropometry, physical capacity, rowing kinematics and rowing performance. *Sports Biomech.*, 2004, **3**, 221–235.
4 **Caplan, N.** and **Gardner, T. N.** The influence of stretcher height on the mechanical effectiveness of rowing. *J. Appl. Biomech.*, 2005, **21**, 286–296.
5 **Caplan, N.** and **Gardner, T. N.** The influence of a three-week familiarisation period on rowing mechanics at a new stretcher position. *Int. J. Sports Sci. Engng*, 2008, **2**, 15–22.
6 **Pope, D. L.** On the dynamics of men and boats and oars. In *Mechanics and sports* (Ed. J. L. Bleustein), 1973, pp. 113–130 (The American Society of Mechanical Engineers, New York).
7 **Atkinson, W. C.** Rowing computer research, available from http://www.atkinsopht.com/row/rowrpage.htm (accessed 25 May 2009).
8 **Dudhia, A.** Physics of rowing, available from http://www.atm.ox.ac.uk/rowing/physics/ (accessed 25 May 2009).
9 **van Holst, M.** On rowing, available from http://home.hccnet.nl/m.holst/RoeiWeb.html (accessed 25 May 2009).
10 **Caplan, N.** and **Gardner, T.** Modeling the influence of crew movement on boat velocity fluctuations during the rowing stroke. *Int. J. Sports Sci. Engng*, 2007, **1**, 165–176.
11 **Hill, H.** and **Fahrig, S.** The impact of fluctuations in boat velocity during the rowing cycle on race time. *Scand. J. Med. Sci. Sports*, 2009, **19**, 585–594.
12 **Formaggia, L., Miglio, E., Mola, A.,** and **Montano, A.** A model for the dynamics of rowing boats. *Int. J. Numer. Methods Fluids*, 2009, **61**, 119–143.
13 **Berton, M., Alessandrini, B., Barré, S.,** and **Kobus, J. M.** Verification and validation in computational fluid dynamics: application to both steady and unsteady rowing boats numerical simulations. In Proceedings of the 16th International Offshore and Polar Engineering Conference, Lisbon, Portugal, 1–6 July 2007.
14 **Berton, M., Alessandrini, B., Barré, S.,** and **Kobus, J. M.** Hydrodynamic analysis of the performance of rowing boats with unsteady motions. In Proceedings of the Numerical Towing Tank Symposium, Le Croisic, France, 2006.
15 **Berton, M.** *Analyse et optimisation numériques des performances de carènes élancées en mouvement instationnaire, application aux bateaux d'aviron*. PhD Thesis, Ecole Centrale de Nantes et Université de Nantes, 2007.
16 **Wellicome, J. F.** Some hydrodynamique aspects of rowing. In *Rowing, a scientific approach* (Eds J. G. P. Williams and A. C. Scott), 1967, pp. 22–63 (Kaye and Ward, London).
17 **Cabrera, D., Ruina, A.,** and **Kleshnev, V.** A simple 1^+ dimensional model of rowing mimics observed forces and motions. *Hum. Move. Sci.*, 2006, **25**, 192–220.
18 **Leroyer, A., Barré, S., Kobus, J. M.,** and **Visonneau, M.** Experimental and numerical investigations of the flow around an oar blade. *J. Marine Sci. Technol.*, 2008, **13**, 1–15.
19 **Kinoshita, T., Miyashita, M., Kobayashi, H.,** and **Hino, T.** Rowing velocity prediction program with estimating hydrodynamic load acting on an oar blade. In Proceedings of the Third International Symposium on Aero Aqua Bio Mechanisms (ISABMEC), Okinawa, Japan, 2006.
20 **Hase, K., Kaya, M.,** and **Yamazaki, N.** Development of three-dimensional whole-body musculoskeletal model for various motion analyses. *JSME Int. J., Série C*, 1997, **40**, 25–32.
21 **Hase, K., Kaya, M., Yamazaki, N., Andrews, B., Zavatsky, A.,** and **Halliday, S.** Biomechanics of rowing (I. A model analysis of musculo skeletal loads in rowing for fitness). *JSME Int. J., Série C*, 2002, **45**, 1073–1081.
22 **Hase, K., Kaya, M., Yamazaki, N., Andrews, B., Zavatsky, A.,** and **Halliday, S.** Biomechanics of rowing (II. A control model for the simulation study of rowing and other human movement). *JSME Int. J., Série C*, 2002, **45**, 1082–1092.
23 **Hase, K., Kaya, M., Zavatsky, A.,** and **Halliday, E.** Musculoskeletal loads in ergometer rowing. *J. Appl. Biomech.*, 2004, **20**, 317–323.
24 **Zatsiorsky, V.** and **Seluyanov, V.** The mass and inertia characteristics of the main segments of the human body. In *Biomechanics VIII-B* (Eds H. Matsui and K. Kobayashi), 1983, pp. 1152–1159 (Human Kinetics, Champaign, Illinois).
25 **Cheng, H., Obergefell, L.,** and **Riser, A.** Generator of body (GEBOD) manual report, AL/CF-TR-1994–0051, Armstrong Laboratory, Wright-Patterson Air Force Base, 1994.
26 **Cheng, H., Obergefell, L.,** and **Riser, A.** Development GEBOD program. In Proceedings of the 15th Southern Biomedical Conference, Dayton, Ohio, 29–31 March 1996.
27 ITTC Recommended procedures and guidelines available from http://ittc.sname.org/2006_recomm_proc/7.5-02-02-01.pdf (accessed 25 May 2009).
28 **Barré, S.** *Etude expérimentale des systèmes de propulsion instationnaire. Application aux palettes d'aviron*. PhD Thesis, Ecole Centrale de Nantes et Université de Nantes, 1998.
29 **Scragg, C. A.** and **Nelson, B. D.** The design of an eight-oared rowing shell. *Marine Technol.*, 1993, **30**(2), 84–99.

APPENDIX

On-water measurements

The horizontal oar angles were measured with high precision potentiometers (Novotechnik P1411). The global accuracy was about ±0.5°. The seat position was measured with a seat slide equipped with two pulleys and an endless timing belt which drove a potentiometer (Megatron A05). The accuracy was about ±3 mm. The boat velocity was measured by a sensor fixed on the boat fin. This sensor was composed of a ducted Schiltknecht micro propeller and a magnetic micro switch which counted the passage of the propeller blades. This sensor had a high dynamical response and its accuracy was about

±0.02 m/s. It was calibrated in a towing tank on the skiff.

The pitch and heave movements of the boat were obtained with two accelerometers (Entran EGCS 5g), one fixed on the aft part of the boat, the other on the fore part at a known distance. The accelerometers measured the vertical accelerations which were used to calculate the heave acceleration and the pitch angular acceleration. Those quantities were integrated to obtain the heave and the pitch movement. The calculations were facilitated by the fact that the pitch and heave and their derivatives all had zero means. The measurements were centralized in a light data logger (IRAAM CC3).